Electric field-induced plasma convection in tokamak divertors

J. A. Boedo,[a] M. J. Schaffer, R. Maingi,[b] and C. J. Lasnier[c]
General Atomics, P.O. Box 85608, San Diego, California 92186-5608

(Received 13 September 1999; accepted 3 January 2000)

Measurements of the electric fields, **E** in the DIII-D tokamak divertor region [J. C. Luxon and L. G. Davis, Fusion Technology **8**, Part 2A, 441 (1985)] are quantitatively consistent with recent computational modeling establishing that $\mathbf{E}\times\mathbf{B}_T$ circulation is the main cause of changes in divertor plasmas with the direction of the toroidal magnetic field, $\mathbf{B}_T$. Extensive two-dimensional measurements of plasma potential in the DIII-D tokamak divertor region are reported for the first time. The resulting $\mathbf{E}\times\mathbf{B}_T/B^2$ drift particle flux is calculated for standard (ion $\nabla\mathbf{B}_T$ drift toward divertor *X*-point) and reversed $\mathbf{B}_T$ direction and for low (*L*) and high (*H*) confinement modes. Perpendicular field strengths of up to $\mathbf{E}\sim 5$ kV/m are observed at the separatrix between the divertor private region and the scrape-off layer (SOL). The $\mathbf{E}\times\mathbf{B}_T$ drift, which reverses with reversal of $\mathbf{B}_T$, creates a poloidal circulation pattern in the divertor that convects 25%–40% of the total ion flow to the divertor target. The circulation strongly couples the various regions of the divertor and SOL and fuels the *X*-point region. An outward shift of the profiles is seen in reversed $\mathbf{B}_T$. © *2000 American Institute of Physics.* [S1070-664X(00)01104-6]

A magnetic divertor in a tokamak provides heat and particle exhaust and shields the main plasma from impurity contamination. Heat and particles are transported from the plasma core (Fig. 1) to the edge and scrape-off layer (SOL) plasma, where the particles are convected and the heat is conducted and convected to the divertor. The SOL transport is mainly parallel to the magnetic-field **B**. The heat and particle fluxes impinge on the divertor targets, where impurities are released from plasma-facing components. Thus, it is important to understand divertor physics,[1] particularly plasma flows,[2–4] that can affect divertor operation and design.

Of special interest is the unexplained observation that asymmetries in the power and particle distributions between the inner and outer divertor targets are sensitive to the direction of the toroidal magnetic-field $\mathbf{B}_T$.[5] Power fluxes between the inner and outer targets differ by factors of five or more with one $\mathbf{B}_T$ direction, yet the difference can nearly disappear when $\mathbf{B}_T$ is reversed. It has been hypothesized that this asymmetry arises in some way from the $\mathbf{B}\times\nabla B/B^2$ and $\mathbf{E}\times\mathbf{B}/B^2$ particle drifts, where **E** and **B** are the electric and magnetic-field vectors.[5] $\mathbf{E}\times\mathbf{B}$ poloidal particle drifts are observed in the SOL of many plasma devices, and two-dimensional (2D) measurements of these have been made in the Continuous Current Tokamak (CCT),[6,7] a nondiverted tokamak. Due to the dominance of $\mathbf{B}_T$ in tokamaks, the drifts change direction with $\mathbf{B}_T$. Recent numerical calculations with the UEDGE plasma and gas simulation code, including all the classical particle drifts, reproduce the main features of the in–out asymmetry dependence on $\mathbf{B}_T$ direction.[8] By enabling or disabling the various drift terms in the UEDGE code, the $\mathbf{E}\times\mathbf{B}$ drift was identified as dominant, in agreement with theoretical prediction.[5] Most theoretical and experimental divertor research to date has concentrated on plasma transport parallel to the magnetic field which, being independent of the direction of $\mathbf{B}_T$, cannot explain the experimental results. This letter reports first experimental measurements of divertor electric fields, the corresponding calculated flows in the private region, and confirms computational predictions. The drifts discussed here are a universal phenomenon, arising from electron temperature and density gradients, and are, therefore, a general feature of edge, SOL, and divertor plasmas.

The electric drift velocity for ions and electrons in a tokamak is

$$\mathbf{v}_E=\mathbf{E}\times\mathbf{B}/B^2=-\nabla\Phi\times\mathbf{B}/B^2\approx-\nabla\Phi\times\mathbf{B}_T/B_T^2, \qquad (1)$$

where Φ is the scalar electric potential. The divergence-free part of the diamagnetic or $\mathbf{B}\times\nabla p/B^2$ velocity is not a true drift and transports no ions or energy,[9] while the guiding center drift component, a true drift, is of minor importance.[8] Therefore, the diamagnetic drift is not considered here.

The experiments were carried out in the DIII-D tokamak[10] with plasma current $I_p=1.4$ MA, $B_T=2.1$ T at $R_o=1.7$ m. The neutral beam heating power varied from 0.5 to 8.75 MW during the discharge, producing low (*L*) and high (*H*) mode phases. The single-null divertor is in the bottom of the vacuum vessel, which is instrumented for divertor studies.[1] Standard and reversed $\mathbf{B}_T$ directions were compared. Conditions were successfully chosen to eliminate the additional complications of divertor detachment and parallel gradients, as we show later.

The principal measurements were made by a fast scanning probe array featuring five tips used to measure ion saturation current, electron temperature T_e, electron density n_e, floating potential Φ_f and the parallel plasma Mach number in the divertor. The plasma potential Φ_p was calculated from Φ_f and T_e. The probe scans vertically from the divertor plate in ~250 ms along the path indicated in Fig. 1 at major radius $R=1.48$ m. The divertor Thomson scattering system, also at $R=1.48$ m, provided independent T_e and n_e measurements at eight locations separated by 2 to 3 cm every 50 ms. The divertor plasma was stepped in major radius by

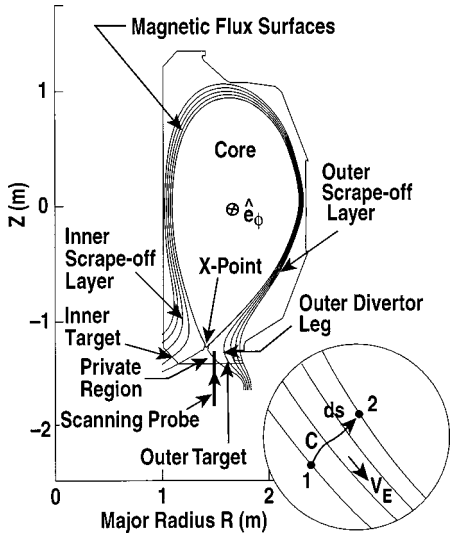

FIG. 1. Poloidal cut of a DIII-D diverted discharge showing major plasma and geometrical features.

changing the external equilibrium magnetic field to obtain 2D measurements over most of the divertor region. The measurements taken along the various probe insertions [Fig. 2(a) inset] are mapped on to the magnetic surfaces calculated by the toroidal equilibrium fitting code EFIT[11] to form a composite plot. The magnetic surfaces are labeled by their normalized poloidal magnetic flux, ψ_n. The separatrix is at $\psi_n=1$; $\psi_n>1$ is the SOL with ψ increasing away from the separatrix; and $\psi_n<1$ is either private region or core plasma with ψ_n decreasing away from the separatrix.

Results are shown in Fig. 2 for standard $\mathbf{B}_T$ ELMing (edge-localized mode) *H*-mode discharges for the outer SOL region. The potential [Fig. 2(a)] rises by ~200 V from the cold private region to the hot separatrix over 4 to 5 cm (5 kV/m), followed by a decrease through the SOL (~1 kV/m) as T_e decreases [Fig. 2(c)]. The potential ''well'' seen in Fig. 2(d) just outside the separatrix is a reproducible feature; although not important to our main argument, it is qualitatively consistent with the measured current to the target and the $J_\parallel/\sigma_\parallel$ term in Eq. (2) below. This well feature results in larger gradients (7 kV/m) and a double velocity shear layer. The plotted traces are composites from the probe trajectories shown in inset of Fig. 2(a). The fact that potential data taken along different trajectories (various symbols in Fig. 2) overlay well when plotted as a function of magnetic flux alone means that the parallel potential gradients are within the data scatter in these particular divertor plasmas. Therefore, the potential gradients in Fig. 2(a) yield the normally directed electric field. The measured variation of Φ_p is not due to parallel pressure or temperature gradients in the plasma, but to the sheath potential and its dependence on T_e. The measured potentials jump up by the sheath potential when the scanning probe, which normally rests below the target surface, first meets plasma.

The inner SOL potential variation with flux surface [Fig. 3(a)] is, out to the last measured flux surface, nearly the same as the outer. We find that for reversed $\mathbf{B}_T$ the potential change is again ~200 V [Fig. 3(c)], but the outer profiles are slightly shifted outwards [Figs. 3(c) and 3(d)]. This is due to the radial drift caused by the poloidal electric field, as predicted by the simulation.[8]

The potential on magnetic lines intersecting an electrically conducting target is determined by the electron parallel momentum equation (or plasma parallel Ohm's law), valid in the short mean-free path limit,[12] and without kinetic effects

$$-E_\parallel=\nabla_\parallel\Phi=\frac{\nabla_\parallel n_e T_e}{n_e}+0.71\nabla_\parallel T_e-\frac{J_\parallel}{\sigma_\parallel}, \tag{2}$$

where $J_\parallel$ is parallel electric current and $\sigma_\parallel$ is parallel electrical conductivity. Starting from $\Phi=0$ at the target, the potential rises mainly by the large density change across the very thin sheath in front of the target (for constant T_e) in accordance with $\nabla_\parallel\Phi\approx T_e\nabla_\parallel\ln n_e$. The theory of sheaths with grazing magnetic field[13] gives $\Phi\approx 3\,T_e$ for hydrogen plas-

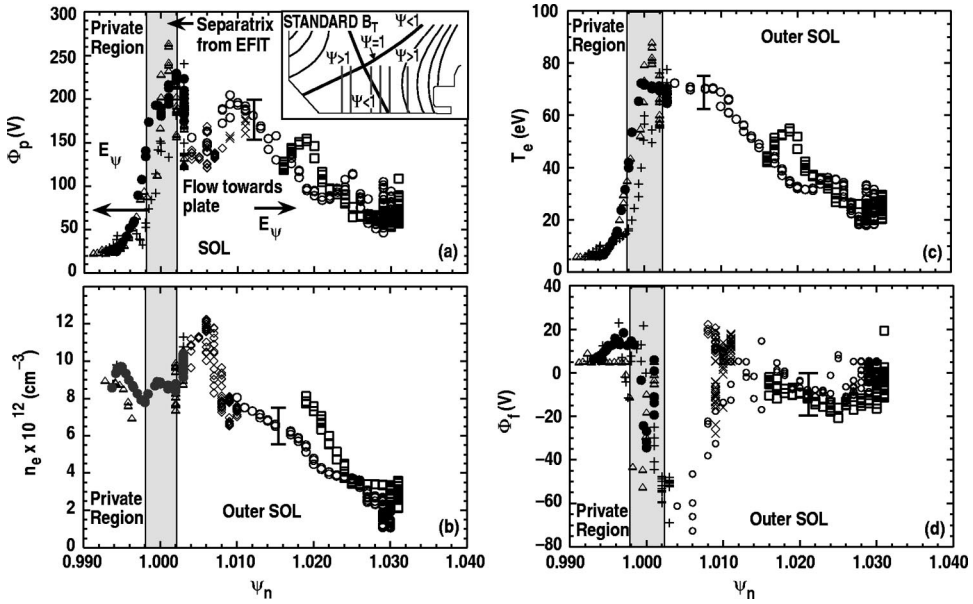

FIG. 2. Standard B_T: Measured (a) Φ_p profile, (b) n_e profile, (c) T_e profile, and (d) Φ_f profile as a function of ψ at the outer divertor leg. Probe trajectories used to make the composite plots are shown schematically in the inset in (a). The traces overlay well, indicating that parallel gradients are negligible.

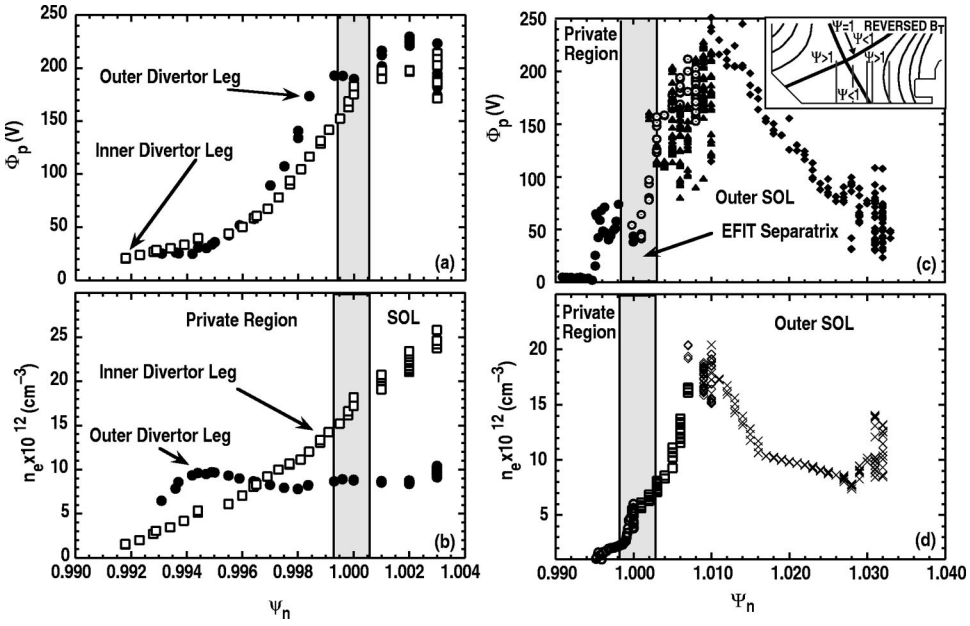

FIG. 3. Standard B_T: Measured (a) Φ_p profile and (b) n_e profile at the inner and outer divertor legs. Reversed B_T: Measured (c) Φ_p profile and (d) n_e profile. The inset on (c) shows the probe trajectories used to build the composite plots.

mas. In the present experiments neither T_e nor n_e vary strongly along a given magnetic line once into the plasma. Thus, the potential gradient in the divertor plasma, $-\nabla\Phi$, is mainly normal to the magnetic surfaces.

Equation (1) then yields a plasma drift along the magnetic surfaces in the poloidal direction in the SOL and the private region, shown in Fig. 4. The result is plasma circulation from one divertor leg and target to the other. We stress the $\mathbf{E}\times\mathbf{B}_T$ ion flow along the private flux side of the separatrix, which has been ignored until recently.[8]

The number of particles per second $\dot{N}$ convected poloidally by the drift velocity $\mathbf{v}_E$ through a surface defined by the rotation of a curve C, connecting flux surfaces containing points 1 and 2, about the major radius axis (Fig. 1 inset) is

$$\dot{N}\approx\int_1^2 2\pi Rn(d\mathbf{s}\times\mathbf{v}_E)\cdot\hat{e}_\phi\approx 2\pi\int_1^2\frac{Rn}{B_T}(\nabla\Phi)\cdot d\mathbf{s}$$
$$=2\pi\int_{\Phi_1}^{\Phi_2}\frac{Rn}{B_T}d\Phi, \qquad (3)$$

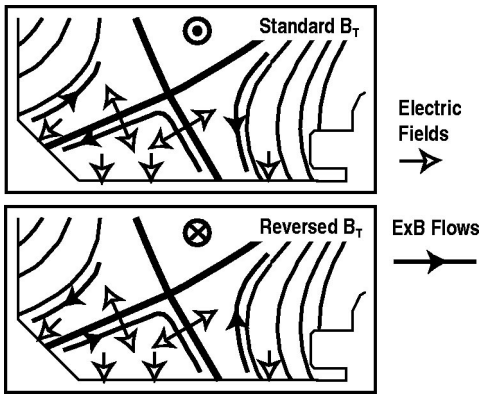

FIG. 4. Schematic electric field and $\mathbf{E}\times\mathbf{B}$ drift directions in the divertor region for standard and reversed B_T.

where Φ_1 and Φ_2 are the potentials at points 1 and 2. If B_T, R and n are all nearly constant across the potential gradient region, Eq. (3) simplifies to

$$\dot{N}\approx 2\pi Rn(\Phi_1-\Phi_2)/B_T, \qquad (4)$$

and $\dot{N}$ depends on just the potential difference across the plasma flow layer. For standard $\mathbf{B}_T$, the electron density across the private region potential gradient region is fairly constant at $\approx 1\times10^{19}\,\mathrm{m}^{-3}$, Fig. 2(b), and use of Eq. (4) is justified. Then the calculated private poloidal ion flow is $\dot{N}\approx 1\times10^{22}\,\mathrm{s}^{-1}$. The ion flow to the outer target for these discharges was measured by target mounted probes to be $\approx 2\times10^{22}\,\mathrm{s}^{-1}$ and ion flow to the inner target was $0.7-2\times10^{22}\,\mathrm{s}^{-1}$. Thus, the private poloidal $\mathbf{E}\times\mathbf{B}$ ion flow is $\sim$25%–40% of the total (inner plus outer) target ion flow, and is comparable to the inner target flow. The private poloidal flow for reversed B_T is comparable in magnitude but reversed in direction. The private poloidal ion flow is supplied by radial diffusion. The SOL poloidal $\mathbf{E}\times\mathbf{B}$ flow is of strength ($\sim 6\times10^{21}$) comparable to the private region poloidal flow and directed as shown in Fig. 4.

The L-mode discharges, not shown, showed similar features. The potential difference across the separatrix was lower, $\sim$125 V. The private poloidal $\mathbf{E}\times\mathbf{B}$ ion flow was $\dot{N}\sim 1\times10^{22}\,\mathrm{s}^{-1}$, and the total target ion flow was $\sim 2\times10^{22}\,\mathrm{s}^{-1}$.

A consequence of the existence of the poloidal flows is their effect on the (deuterium) ion flux to the target. The poloidal velocity is of the order of 1 to 2×10^3 m/s, whereas the parallel velocity at the separatrix is of the order of $0.5-1\times10^4$ m/s far from the target and $\sim 3\times10^4$ m/s at the target.[4] The poloidal velocity is large enough to affect the magnitude and direction of the net flow, preventing it from following the magnetic-field lines. In these experiments, for standard $\mathbf{B}_T$, the parallel flow at the inner strike point

reaches the target at $\sim 0.5^0$ steeper angle than the parallel magnetic field (1.5^0) whereas at the outer strike point it is shallower.

The particle flux associated with the velocity $\mathbf{v}_E$, convects a heat flux as power Braginskij[12]

$$q_E = n_i \mathbf{v}_E e\{\tfrac{5}{2}[T_i + (n_e/n_i)T_e] + \Phi_I\}, \quad (5)$$

with the addition of Φ_I, which is the ionization potential. This equation can be integrated across the potential gradient like Eq. (3), and for approximately uniform $T_e = T_i$ (from spectroscopy and Thomson) and $n_e = n_i$, the convected heat flow is $Q_E = \dot{N}e(5T_e + \Phi_I)$. For the standard B_T discharge, if we approximate T_e by 20 eV and let $\Phi_I = 13.6$ eV (deuterium), the poloidal private heat flow is ~ 0.2 MW. Measurements of heat flux to the targets by an IR (infrared) camera show a total of 1.43 MW deposited onto the targets. Thus, the poloidal private flow is not important globally. However, $q_E \approx 0.48\ \mathrm{MW/m^2}$ is calculated just on the private side of the separatrix, which is comparable to IR camera measurements of peak heat fluxes to the inner and outer targets of 0.5 and 1.4 $\mathrm{MW/m^2}$, respectively. Therefore, q_E can be important locally.

The strength of the measured $\mathbf{E}\times\mathbf{B}$ flow and the agreement between computational modeling and experiment establishes that $\mathbf{E}\times\mathbf{B}/B^2$ drift poloidal circulation is the main cause of the long-observed changes in divertor plasmas with the direction of $\mathbf{B}_T$. The UEDGE simulation showed private ion poloidal $\mathbf{E}\times\mathbf{B}$ flow of $0.51\times 10^{22}\,\mathrm{s^{-1}}$, for standard B_T direction and $0.69\times 10^{22}\,\mathrm{s^{-1}}$ for reversed $\mathbf{B}_T$, similar to the experimental values. These UEDGE simulations included cross-B drifts, not included in standard 2D simulations, however they did not include impurity effects, a fact that allowed a clear identification of the drift effects. Our results emphasize the need to include electric fields and drifts self-consistently in divertor modeling, both for interpretation of experimental measurements and for prediction of future divertor performance.

This research was supported by the U.S. Department of Energy under Contract Nos. DE-AC03-99ER54463, W-7405-ENG-48, DE-AC05-96OR22464, DE-AC04-94AL85000, and Grant No. DE-FG03-95ER54294. Discussions with T.D. Rognlien, G.D. Porter, and S.L. Allen and the assistance of R.D. Lehmer and R.A. Moyer are acknowledged.

[a]Also at: University of California, San Diego, San Diego, California. Electronic mail: jboedo@fusion.ucsd.edu
[b]Also at: Oak Ridge National Laboratory, Oak Ridge, Tennessee.
[c]Also at: Lawrence Livermore National Laboratory, Livermore, California.

[1]C. S. Pitcher and P. C. Stangeby, Plasma Phys. Controlled Fusion **39**, 779 (1997).
[2]N. Asakura, S. Sakurai, N. Hosogane, K. Itami *et al.*, 17th IAEA Fusion Energy Conference, Yokohama (1998), Nucl. Fusion (to be published).
[3]M. J. Schaffer *et al.*, Nucl. Fusion **35**, 1000 (1995).
[4]J. A. Boedo, G. D. Porter, M. J. Schaffer *et al.*, Phys. Plasmas **5**, 4305 (1998).
[5]A. V. Chankin *et al.*, Plasma Phys. Controlled Fusion **36**, 1853 (1994).
[6]G. Tynan, Dissertation, UCLA School of Engineering and Applied Science (1991).
[7]G. R. Tynan, J. Liberati, P. Pribyl, R. J. Taylor, and B. Wells, Plasma Phys. Controlled Fusion **38**, 1301 (1996).
[8]T. D. Rognlien, G. D. Porter, and D. D. Ryutov, J. Nucl. Mater. **266-269**, 654 (1999).
[9]A. V. Chankin, J. Nucl. Mater. **241-243**, 199 (1997).
[10]J. C. Luxon and L. G. Davis, Fusion Technol. **8**, 441 (1985).
[11]L. L. Lao *et al.*, Nucl. Fusion **25**, 1611 (1985).
[12]S. I. Braginskii, *Reviews of Plasma Physics*, edited by M. A. Leontovich (Consultants Bureau, New York, 1965), Vol. 1, p. 205.
[13]R. Chodura, Phys. Fluids **25**, 1628 (1982).